Bull. Mater. Sci., Vol. 34, No. 3, June 2011, pp. 477–482. © Indian Academy of Sciences.

Preparation and characterization of solid-state sintered aluminum-doped zinc oxide with different alumina contents

YU-HSIEN CHOU*, J L H CHAU, W L WANG, C S CHEN, S H WANG and C C YANG
Nanopowder and Thin Film Technology Centre, ITRI–South, Industrial Technology Research Institute, Tainan 70955, Taiwan

MS received 23 August 2010; revised 1 March 2011

Abstract. **Aluminum-doped zinc oxide (AZO) ceramics with 0−2·5 wt.% alumina (Al_2O_3) content were prepared using a solid-state reaction technique. It was found that AZO grains became finer in size and more irregular in shape than undoped ZnO as the Al_2O_3 content increased. Addition of Al_2O_3 dopant caused the formation of phase transformation stacking faults in ZnO grains. The second phase, $ZnAl_2O_4$ spinel, was observed at the grain boundaries and triple junctions, and inside the grains. In this study, a 3-inch circular Al_2O_3 (2 wt.%)-doped ZnO ceramic target sintered at 1500°C for 6 h has a relative density of 99·8% with a resistivity of $1{\cdot}8 \times 10^{-3}\Omega$-cm. The AZO film exhibits optical transparency of 90·3% in the visible region and shows an electrical resistivity of $2{\cdot}5 \times 10^{-3}\Omega$-cm.**

Keywords. **AZO target; $ZnAl_2O_4$ spinel; resistivity; AZO thin film.**

1. Introduction

Transparent conducting oxides (TCOs) have received considerable attention in recent years due to their good transparency and high electrical conductivity. They have broad range of applications such as transparent electrodes in solar cells and liquid crystal displays (LCDs) (Sharma and Exarhos 1995). Most of the TCOs are based on indium oxide (In_2O_3), zinc oxide (ZnO), tin oxide (SnO_2), and their mixed compounds (Chopra *et al* 1983; Coutts *et al* 2000).

ZnO is naturally an *n*-type semiconductor material. Due to its wide direct bandgap (∼3·3 eV), its transmittance in the visible region is extremely high (Chopra *et al* 1983). ZnO has attracted interest as an alternative transparent conducting material to indium tin oxide (ITO) because of its (i) low cost, (ii) low growth temperature, (iii) non-toxicity, and (iv) easy adjustment of conductivity by adding impurities, such as Al, Sb and Mn (Han *et al* 2001a; Zhang *et al* 2006). Many techniques have been developed for the deposition of Al-doped ZnO (AZO) thin films, e.g. chemical vapour deposition (Tominaga *et al* 1999), wet-coating (Chatelon *et al* 1997), and RF-magnetron sputtering (Jeong *et al* 2003; Ben Ayadi *et al* 2008). Sputtering is a mature technology and has been extensively used for today's display applications. For the deposition of a high quality AZO thin film on a substrate via sputtering, a target with high sintering density is required.

In this work, preparation of high quality AZO targets doped with 0−2·5 wt.% alumina (Al_2O_3) content using a solid-state reaction method was investigated. We studied the effects of Al_2O_3 dopant on the electrical resistivity, densification, and grain growth. A dense and low electrical resistivity of AZO (Al_2O_3: 2 wt.%) target with a diameter of 3 inch was used for the deposition. The transparent conducting thin film was deposited at room temperature by RF-magnetron sputtering. The structure, optical and electrical properties of the sputtered AZO thin film were analysed by X-ray diffraction, UV-visible spectrum and Hall effect measurement, respectively.

2. Experimental

The Al-doped ZnO ceramics was synthesized via solid-state reaction of ZnO (99·9%, Aldrich, Milwaukee, WI) and Al_2O_3 (99·9%, Showa, Tokyo, Japan) powders. The mean particle sizes of ZnO and Al_2O_3 powders are 75 μm and 40 nm, respectively. The ZnO powders were thoroughly mixed with different amounts of Al_2O_3 by ball-milling with ethanol using yttria-stabilized ZrO_2 (YSZ) balls in a polyethylene (PE) bottle for 24 h. The amounts of Al_2O_3 dopant in the samples were 0, 1·5, 2·0, and 2·5 wt.%. The mixed slurry and YSZ balls were separated by sieving through 74 μm mesh, and slurry was put into the oven to remove the solvent. After drying at 100°C for 24 h, powders were ground using an agate mortar and pestle and deagglomerated by sieving through a 37 μm mesh. The powders were then die-pressed into discs of 12 mm (ϕ) and 3 mm thick using a WC-inserted steel die at a uniaxial pressure of 40 MPa. The green density of the compacts was around 49 ± 1% calculated from the weight and dimensions of the green compacts.

*Author for correspondence (yuhsienchou@itri.org.tw)

Table 1. Sputtering parameters of deposited AZO thin film.

Sputtering parameters	Conditions
Power (RF)	200
Base pressure	3×10^{-6} Torr
Working pressure	5 m Torr
Substrate (temperature)	Room temp.
Target to substrate distance	7 cm
Ar flow	20 sccm
Film thickness	about 600 nm

The discs were then sintered in air at 1500°C for 6 h with a heating and cooling rate of 5°C/min. The as-sintered bulk density was measured by the Archimedes method. After mechanical grinding, sintered samples were then oxide polished to ∼50 nm surface roughness. Polished sections were chemically etched in a 5%HCl solution to delineate grains and domain boundaries. The morphologies of AZO powders and microstructures of the sintered bulk were observed using a field-emission gun SEM (JEOL^{TM} 6330, Tokyo, Japan). Transmission electron microscopy (TEM, JEOL^{TM} AEM 3010, Tokyo, Japan) was performed to observe the secondary phase and microstructure of sintered specimens. The crystalline phases of sintered samples were identified via X-ray diffractometry (XRD) using a Siemens D5000 diffractometer (Karlsruhe, Germany), with Cu$K\alpha_{1+2}$ radiation operating at 40 kV/30 mA.

A 3-inch circular sputtering target made by 2 wt.% alumina doped ZnO was used for thin film deposition. The as-prepared powder was disc-formed into a diameter of 100 mm (ϕ) using a uniaxial pressure of 40 MPa. The green density was further improved to 57 ± 0·6% after conducting cold isotatic pressing (CIP) of the compact powders with a pressure of 300 MPa. Then, the disc was sintered with the same sintering condition as previously described. The AZO transparent conductive thin films were deposited on the glass substrates (EAGLE^{2000}, Corning) by an RF-magnetron sputtering system. The distance between sputter target and substrate was kept at 7 cm to ensure uniformity of AZO films. The sputtering conditions are listed in table 1. Hall measurement (Lake Shore 7500/9500 Series Hall System) was employed to measure the resistivity, carrier density and Hall

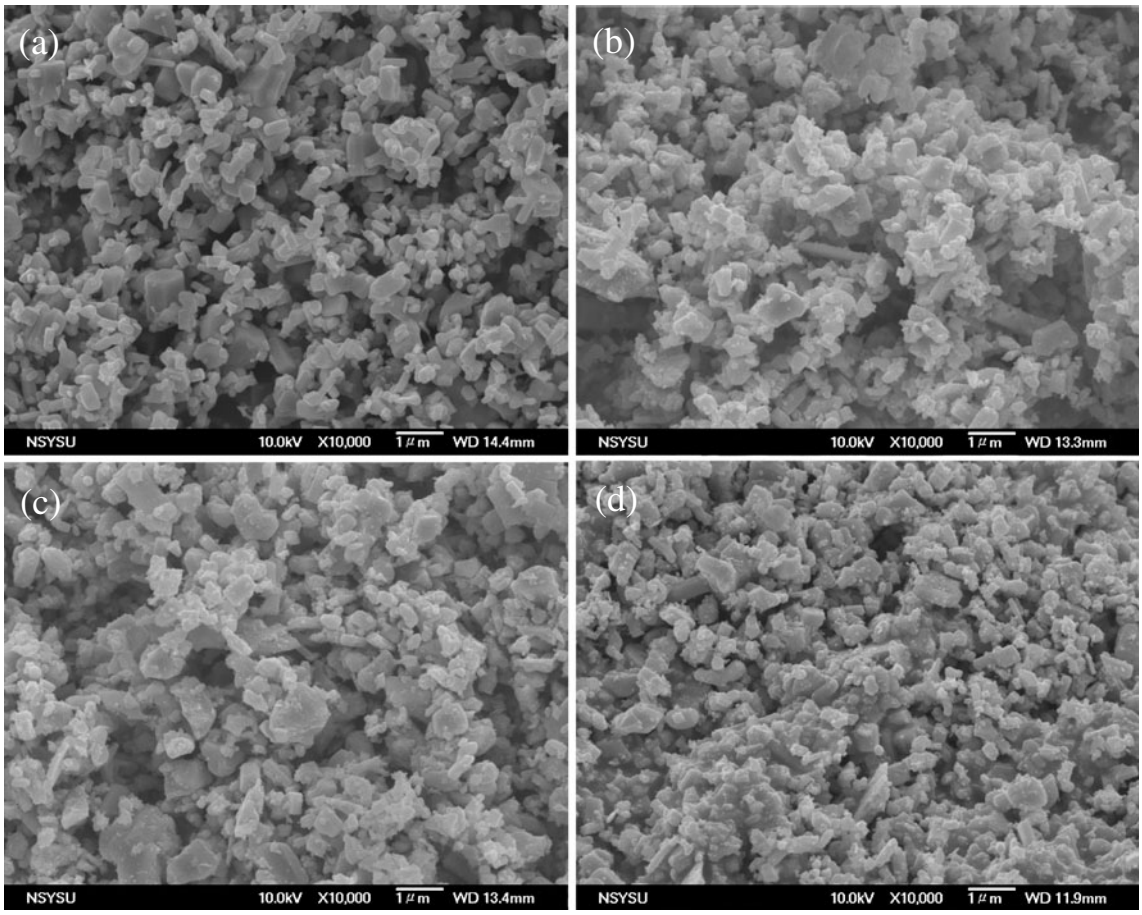

Figure 1. FE–SEM images of as-milled powders: (a) pure ZnO, (b) doped, Al_2O_3 = 1·5wt%, (c) doped, Al_2O_3 = 2wt% and (d) doped, Al_2O_3 = 2·5wt%.

mobility of Al_2O_3 doped ZnO bulk and thin film specimens at 25°C. The optical transmittance of AZO films was measured using a Shimadzu UV 2100 double-beam spectrophotometer.

3. Results and discussion

3.1 *Preparation and characterization of AZO powder and sintering bulks*

Figure 1 (SEM) shows surface morphology of the as-milled ZnO and ZnO with Al_2O_3 contents of 1·5, 2·0, and 2·5 wt.% powders. We observed that the shape and particle size were independent of Al_2O_3 contents according to SEM analysis. The average particles sizes range from 0·2–1·3 μm.

Microstructures of the ZnO–Al_2O_3 system with various Al_2O_3 contents sintered at 1500°C for 6 h are depicted in figure 2. Figure 2(a) shows the sintered bulk of undoped ZnO, which exhibits equiaxed grains and normal grain distribution. Abnormal grain growth was not detected in those specimens. The grain size ranges from 15–30 μm. Figures 2(b)–(d) indicate that the grain size became finer and more irregular in shape when Al_2O_3 was added. The grain size ranges of 1·5, 2·0, and 2·5 wt.% Al_2O_3 doped specimens were 10–20 μm, 10–15 μm, and 5–10 μm, respectively. As shown in figures 2(b)–(d), there were many small grains observed at grain boundaries or grain triple junctions, and also inside the grain, as indicated by solid arrows. Chemical composition (at.%) of the small grains determined by EDS revealed that they were, in fact, the $ZnAl_2O_4$ spinel second phase (Zn : Al : O = 15·54 : 30·62 : 53·84). The phenomena of grain growth inhibition which occurred in the Al_2O_3 doped specimens was attributed to the formation of $ZnAl_2O_4$ second phase, which leads to particle drag effects and reduces the driving force of boundary mobility (Rahaman 1995; Han *et al* 2001b).

Figures 3(a)–(d) show the XRD patterns of pure ZnO and Al_2O_3-doped ZnO of 1·5, 2·0, and 2·5 wt.% contents, respectively. The second phase of cubic $ZnAl_2O_4$ spinel (indicated by triangle symbol) was present in the doped ZnO specimens. When the Al_2O_3 content was raised from 1·5–2·5 wt%, the relative peak intensity of $ZnAl_2O_4$ spinel phase increased. The ratios of peak intensities of $ZnAl_2O_4$ (101)/ZnO (101) are about 0·023, 0·032, and 0·055 as the Al_2O_3 amount increases from 1·5–2·0 and 2·5 wt.%, respectively. A representative TEM bright-field image is given in

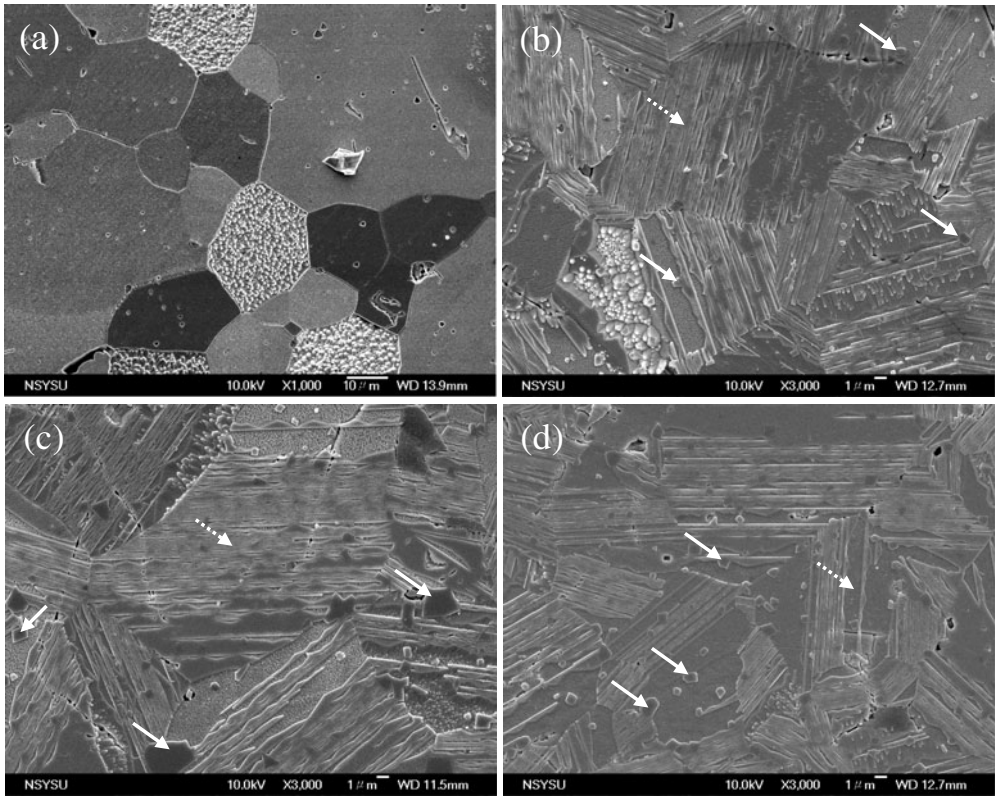

Figure 2. FE–SEM plane-view image of surface morphologies in the ZnO–Al_2O_3 system sintered at 1500°C for 6 h: (**a**) pure ZnO; (**b**) doped, Al_2O_3 = 1·5wt%; (**c**) doped, Al_2O_3 = 2wt%; (**d**) doped, Al_2O_3 = 2·5wt%. (The solid arrow indicates the $ZnAl_2O_4$ spinel second phase and the dotted arrow indicates the ZnO matrix).

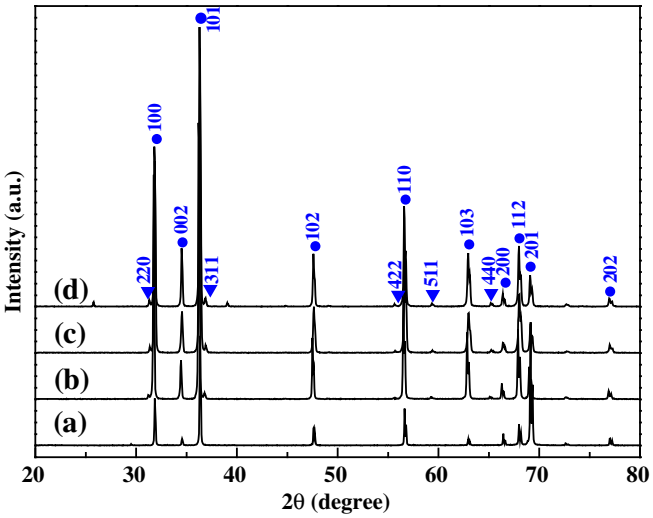

Figure 3. XRD spectra of microstructure in ZnO–Al_2O_3 system sintered at 1500°C for 6 h: (a) pure ZnO; (b) doped, Al_2O_3 = 1·5wt%; (c) doped, Al_2O_3 = 2 wt% and (d) doped, Al_2O_3 = 2·5wt%. (● represents ZnO and ▲ represents $ZnAl_2O_4$ spinel).

figure 4(a), showing that the $ZnAl_2O_4$ spinel second phase existed at grain boundaries. The inhibition of ZnO grain growth resulted from $ZnAl_2O_4$ spinel phase located at grain boundaries or triple junctions, i.e. grain drag effects. Hence, the driving force of boundary mobility was reduced. It was found that residual pores in pure ZnO were mostly trapped in the grains and those in the Al_2O_3-doped ZnO samples were located at grain boundary or triple junctions, as shown in figure 2. The existence of porosity may also induce an electron scattering effect on the electric resistivity.

Table 2 shows the relative density and resistivity of undoped and doped ZnO sintered specimens with various Al_2O_3 contents. Increasing the Al_2O_3 content from 0 to 2 wt.% slightly raises the relative density of ceramic from 99·8%–99·9%. However, the relative density of ceramic with 2·5 wt.% Al_2O_3 addition decreased to 98·4%. The amount of $ZnAl_2O_4$ spinel second phase also increases when the Al_2O_3 content increases to 2·5 wt.% as shown in figure 3. The $ZnAl_2O_4$ spinel second phase located at grain boundaries and triple junctions can induce a grain drag effect and hence reduce the driving force of boundary mobility, i.e. densification of the doped ZnO.

The resistivity decreased from $331{\cdot}1 \times 10^{-3}$ to $1{\cdot}5 \times 10^{-3}\Omega$-cm when the amount of Al_2O_3 was increased to 2 wt.%. The two orders of magnitude reduction of resistivity is due to the trivalent Al ions dissolved in ZnO, which act as a shallow donor (Tang and Cameron 1994). In general, the electrical properties of AZO ceramics are quite related to the microstructures, which might be governed by crystallographic defects, e.g. grain boundary, stacking fault, twin, and dislocation (Sieber *et al* 1998; Lin *et al* 2009; Thonke *et al* 2009; Liu *et al* 2010). The bright-field image (figure 4(b)) shows the dominant crystallographic defect of

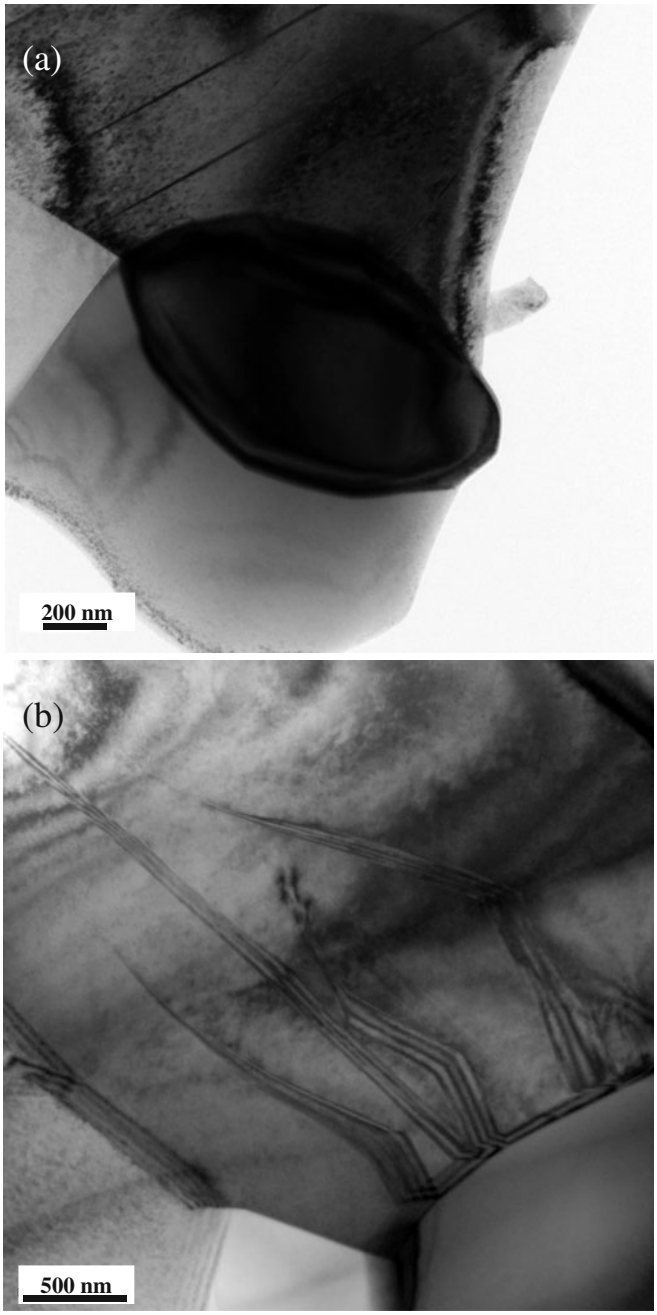

Figure 4. TEM bright-field micrographs of doped-Al_2O_3 ZnO (Al_2O_3, 2 wt%) ceramic sintered at 1500°C for 6 h: (**a**) $ZnAl_2O_4$ spinel and (**b**) stacking faults.

Table 2. Resistivity and relative density of ZnO sintered specimens with various Al_2O_3 contents.

Components	ZnO	ZnO	ZnO	ZnO
Doped-Al_2O_3 (wt %)	0	1·5	2·0	2·5
Resistivity ($\times 10^{-3}\Omega$-cm)	331·1	4·1	1·5	3·5
Relative density (%)	99·8	99·8	99·9	98·4

Figure 5. Photograph of 3-inch AZO ceramic target.

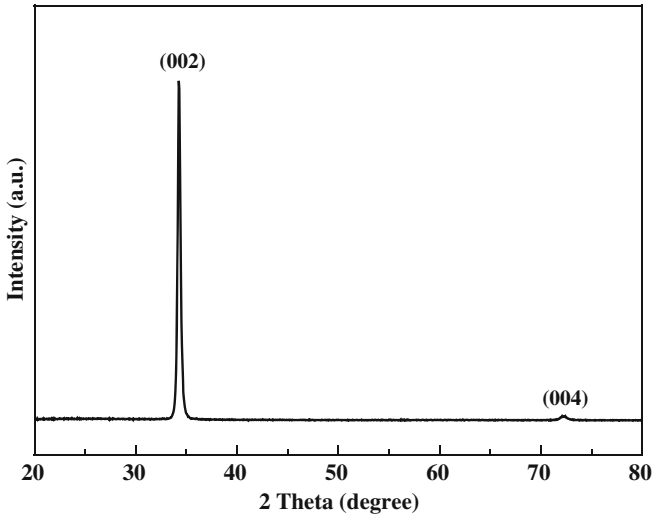

Figure 6. XRD diffraction pattern of AZO thin film.

stacking fault in the Al_2O_3-doped ZnO. It has been reported that the incorporation of group-III or group-V dopants into the matrix apparently increases the tendency to create stacking fault resulting from the dislocation or the lattice misfit (Lin *et al* 2009; Sieber *et al* 1998; Thonke *et al* 2009; Liu *et al* 2010). Compared with the undoped and doped ZnO, the 2·5 wt.% Al_2O_3 doped ZnO has a lower density than the others, indicating that the sintered bulks contain more pores, as shown in figure 2(d). The porosity may result in more electron scattering effect and consequently a high resistivity for the 2·5 wt.% Al_2O_3 doped ZnO.

3.2 *Thin film deposition*

According to the effect of different Al_2O_3 content to the electrical and structural properties of ZnO ceramic, we found that

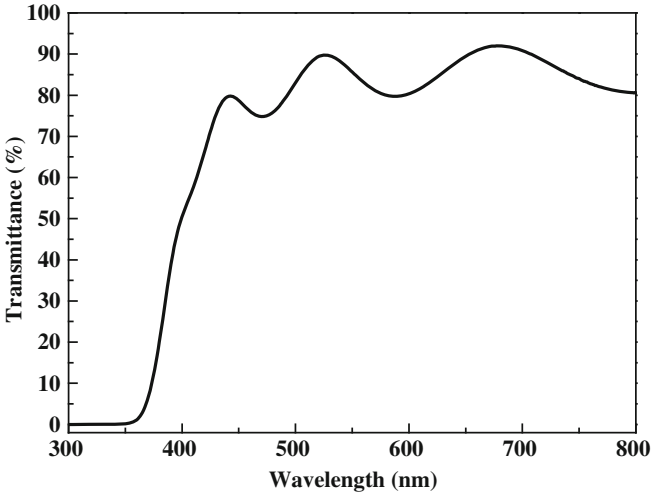

Figure 7. Optical transmittance spectra of AZO thin film.

the 2 wt.% Al_2O_3 doped ZnO target has highest relative density and lowest electrical resistivity. Hence, we use this optimum condition of preparing 3 inch AZO target for thin film deposition.

Figure 5 shows the optical image of the 2 wt.% Al_2O_3-doped AZO target with a diameter of 3 inch. The relative density and resistivity of AZO target were 99·8% and $1{\cdot}8 \times 10^{-3}\Omega$-cm, respectively. Figure 6 illustrates the XRD pattern of AZO film deposited on the glass substrate. The AZO film had a preferred orientation along the (002) direction. Other peak (004) with much less intensity was also observed, indicating that the film has a preferred orientation with their *c*-axis perpendicular to the substrate plane. The grain size of AZO film which was evaluated using the Scherrer's equation is about 29·08 nm. No $ZnAl_2O_4$ spinel second phase was found, implying that Al atoms substitute Zn in the hexagonal lattice and Al ions may occupy the interstitial sites of ZnO. The resistivity, carrier density, and hall mobility of AZO film determined by hall measurement were $2{\cdot}5 \times 10^{-3}$ Ω-cm, $1{\cdot}04 \times 10^{20}$ cm^{-3} and 6·24 cm^2/Vs, respectively. The results revealed that the AZO film is degenerate *n*-type semiconductor. The transmittance of AZO film (the thickness of film is about 500 nm) at 300–800 nm is given in figure 7. The AZO film exhibits an average transmittance of 90·3% in the visible region. According to the results of electrical and optical properties of AZO thin films, it revealed that the 2 wt.% Al_2O_3-doped AZO target can be potentially applied for preparing transparent conductive oxide films. A more detailed study of the relationship between the thin films properties and the deposition parameters are underway.

4. Conclusions

The effects of Al_2O_3 addition on the grain growth, second phase formation, resistivity, and density of ZnO sintered by a solid state reaction technique were studied. The grain

growth inhibition of Al doped-ZnO ceramics is attributed to the formation of $ZnAl_2O_4$ spinel second phase located at the grain boundaries and the grain triple junctions. The resistivity and relative density of the 2 wt.% Al_2O_3-doped AZO target with a diameter of 3 inch were $1{\cdot}8 \times 10^{-3}\,\Omega$-cm and 99·8%, respectively. High transparent and conductive AZO thin film has been obtained by RF magnetron sputtering from this ceramic target. The film demonstrated the optical transparency of 90·3% in the visible region and showed conductivity with electrical resistivity of $2{\cdot}5 \times 10^{-3}\Omega$-cm.

References

Ben Ayadi Z *et al* 2008 *Mater. Sci. Eng.* **C28** 613
Chatelon J P *et al* 1997 *J. Sol-Gel Sci. Technol.* **10** 185
Chopra K L *et al* 1983 *Thin Solid Films* **102** 1
Coutts T J *et al* 2000 *J. Vac. Sci. Technol.* **A18** 2646
Han J, Mantas P Q and Senos A M R 2001a *J. Eur. Ceram. Soc.* **21** 1883
Han J, Mantas P Q and Senos A M R 2001b *J. Mater. Res.* **16** 459
Jeong S *et al* 2003 *Thin Solid Films* **435** 78
Lin J C *et al* 2009 *Thin Solid Films* **517** 4715
Liu K W *et al* 2010 *J. Appl. Phys.* **108** 043516
Rahaman M N 1995 *Ceramic processing and sintering* (New York: Marcel Dekker)
Sharma S K and Exarhos G J 1995 *Thin Solid Films* **270** 27
Sieber I *et al* 1998 *Thin Solid Films* **330** 108
Tang W and Cameron D C 1994 *Thin Solid Films* **238** 83
Thonke K *et al* 2009 *Microelectron. J.* **40** 210
Tominaga K *et al* 1999 *Thin Solid Films* **343–344** 160
Zhang J *et al* 2006 *J. Am. Ceram. Soc.* **89** 3874